Macromolecules

pubs.acs.org/Macromolecules Article

Metallo-Supramolecular Rod−Coil Block Copolymer Thin Films for Stretchable Organic Field Effect Transistor Application

Wei-Ni Wu, Tsung-Han Tu, Chiao-Hsuan Pai, Kuan-Heng Cheng, Shih-Huang Tung, Yi-Tsu Chan,* and Cheng-Liang Liu*

Cite This: *Macromolecules* 2022, 55, 10670−10681 Read Online

ACCESS | Metrics & More | Article Recommendations | Supporting Information

ABSTRACT: Herein, to decrease the synthetic burden of the rod−coil diblock copolymers, the coordination-driven self-assembly approach is utilized to readily construct a series of polystyrene (PS)-*block*-poly(3-hexylthiophene) (P3HT) copolymers with dynamic heteroleptic coordination bonds between the two blocks. In detail, the chain length of the PS is varied for a fixed P3HT chain length to produce block copolymers, namely, PS_{85}−Zn−$P3HT_{187}$ (**P1**) and PS_{161}−Zn−$P3HT_{187}$ (**P2**), with comparable electrical performance to that of homopolymer P3HT (**P0**) in the unstrained state, along with enhanced crack onset strain and much less reduced mobility under 25−100% strain. The ability to maintain the charge transport characteristics is due to the longer coil chain length and amorphous PS regions for the dissipation of strain energy. The organic field effect transistors of **P2** with a longer PS segment show only a slight change in mobility from 5.48×10^{-3} to 1.40×10^{-3} $cm^2\ V^{-1}\ s^{-1}$ under 25−100% and maintain this mobility even after being subjected to 100 repeated stretching/releasing cycles at 50% strain. This proof-of-concept demonstration of the proposed molecular engineering approach based on the metallo-supramolecular method provides a suitable route to the molecular design of stretchable polymer semiconductors with balanced mechanical and electrical behaviors.

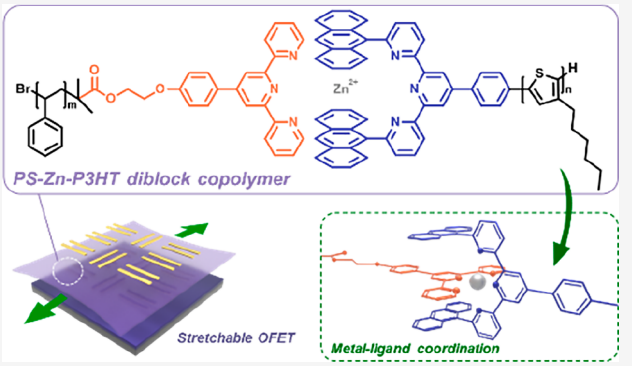

INTRODUCTION

Recent progress in the synthesis and assembly of organic semiconductor materials has established a foundation for electronic devices on flexible, bendable, and stretchable substrates, with various capabilities that cannot be reproduced using conventional Si-based technologies.[1−5] The primary goal of stretchable organic semiconductor electronics is the production of devices with good charge transport properties and performances that are maintained under strain deformation. However, the high mobility (μ) and high degree of crystallinity originate from rigid chains in π-conjugated polymers with an inherent mechanical nonstretchability that is antithetical to deformability. Such brittle semiconductor materials typically require geometric engineering in order to accommodate strain via wrinkled, wavy, and kirigami structures.[6−8] However, while these extrinsic approaches are compatible, they still face the difficulties of limited durability and complicated fabrication. Hence, methods for endowing these organic semiconductor materials with suitable properties for application in high-tolerance, stretchable organic field effect transistor (OFET) devices have become a critical issue. The two main strategies for imparting stretchability to organic semiconductor materials are (i) the fabrication of intrinsically stretchable polymeric semiconductors via delicate molecular design[9−13] and (ii) the fabrication of stretchable semiconducting composites via the physical blending of flexible materials (usually elastomers) into conjugated polymers.[11−15] The general design principle of these two strategies is to lower the crystallinity of the organic semiconductor thin film and to provide the entire film with strain energy dissipation regions under stretching in order to increase its intrinsic deformability.[16]

The electrical and mechanical properties of conjugated polymer semiconductors can be molecularly engineered by modifying the main chain backbone and the side chain in order to control the factors relating to stretchability. The two main approaches to main chain structural design are as follows: (i) inserting flexible conjugation break spacers[17−21] and (ii) inserting twisted backbone structures.[22,23] These approaches enable the backbone flexibility and packing behavior to be directly altered while decreasing the rigidity of the polymers,

Received: May 10, 2022
Revised: November 4, 2022
Published: November 17, 2022

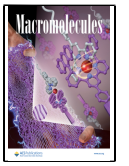

https://doi.org/10.1021/acs.macromol.2c00957
Macromolecules 2022, 55, 10670−10681

thus leading to reduced crystallinity and enhanced softness of the polymeric semiconductor thin film without significantly affecting the μ. When considering side chain engineering, the packing behavior of the thin film can also be manipulated by changing the side chain length/branching characteristics[24−26] and introducing asymmetric[27,28] and specific functional side groups[29−31] via various interchain interactions. Varying these side chain structures has been clearly shown to exert a softening effect upon the conjugated polymer, thereby providing greater ductility and lower elastic modulus while maintaining the charge transport properties. Stretchable composites composed of elastomeric matrices and conjugated polymer chains have also been successfully developed for extrinsic stretchable organic semiconductor materials.[32−37] The polarity difference between these two compounds, and the self-assembly behavior of the conjugated polymers, may facilitate their phase separation to form the semiconducting channel, thereby combining the high charge transport property of the conjugated polymer with the desired mechanical properties of a rubbery polymer. However, to induce thermodynamically stable microscale phase separation and precisely control the distribution of the semiconducting component within the film, an alternative approach is to synthesize block copolymers. In block copolymer systems, two chemically incompatible blocks can self-assemble into different microstructures, leading to various morphologies. The classical microphase separation is generally applied to the coil−coil type block copolymers, in which the Flory interaction parameter χ between the blocks and the block length N, that is, the χ^N value (segregation strength), determines the phase-separated structures, typically forming lamellar, gyroidal, cylindrical, and spherical domains.[38,39] In such cases, the interchain interaction of individual coil block does not play a significant role in the microphase separation. For the rod−coil block copolymers, however, because of the strong $\pi-\pi$ interchain interaction as well as the more stretched, rigid chains of conjugated polymers that tend to firmly pack into crystalline nanofibrils, the microphase separated structure is dominated by rod blocks.[40,41] Despite this, the microstructures of rod−coil block copolymer thin films can still be fine-tuned to optimize their morphologies and corresponding mechanical and electrical properties by applying various combinations of rod and coil blocks.[42]

Recently, several published reports have applied poly(3-hexylthiophene) (P3HT)-based rod−coil block copolymers to the fabrication of stretchable organic transistors.[43−48] Conventionally, the click reaction and Grignard metathesis polymerization have been adopted to synthesize block copolymers.[49−51] However, while such block copolymers have been used to dissipate strain, the development of efficient synthetic approaches toward the facile construction of functional yet diversified rod−coil copolymers remains a formidable challenge. The design of metallo-supramolecular polymers providing an alternative way to synthesize polymers has been studied. Opposite to the convention polymerization methods with the linkage by use of covalent bonds, metallo-supramolecular polymers utilize noncovalent interactions to construct similar properties with the single-chain copolymer.[52] Moreover, metallo-supramolecular polymers have drawn significant attraction as novel functional materials due to their further applications in various fields, for example, stimuli−response, self-healing, shape memory, and light-emitting devices.[53,54] However, only limited studies of metal-coordinated conjugated polymers applied in the OFETs has been reported.[55,56] Herein, a metallo-supramolecular methodology based on predesigned self-selective metal−ligand coordination interactions is utilized to assemble rod and coil segments to afford the desired diblock copolymers. To our knowledge, OFETs based on conjugated diblock copolymers composed using a metallo-supramolecular strategy have not been reported yet. According to our previous study,[57,58] unsubstituted 2,2′:6′,2″-terpyridine (tpy) and 6,6″-di(9-anthracenyl)-substituted tpy are used as end-functionalized groups to ensure precise heteroleptic complexation upon the addition of Zn(II) ions under mild conditions. The rapid construction of diblock copolymers is achieved by taking advantage of these simple metal−ligand coordination complexes. In this work, PS-Zn-P3HT diblock copolymers with variation in the rod/coil block length is fabricated, utilizing self-selective metal coordination between the amorphous polystyrene (PS) coil segment and the semiconducting P3HT rod segment. Further application of stretchable thin-film transistors is also performed to verify the feasibility. The metallo-supramolecular fabrication approach to the block copolymers introduced herein results in a good combination of electrical properties and stretchability.

EXPERIMENTAL SECTION

General Procedure for Complexation. One equivalent of $Zn(OTf)_2$ in MeOH (0.1 M) was added to an equimolar solution of $P3HT_{187}$ (**P0**) and PS_m (m = 85 or 161) in $CHCl_3$. The stoichiometry was verified by ^1H NMR. After the reaction mixture was stirred at room temperature for 5 min, the solvent was evaporated under reduced pressure, and the residue was washed with MeOH to give the corresponding diblock copolymers.

OFET Fabrication and Characterizations. The OFETs with solution-sheared polymer films were fabricated to measure the field effect mobility. A heavily n-doped Si wafer was used as the substrate, with thermally grown 300 nm SiO_2 as a dielectric layer. After sonication in acetone and 2-propanol, the substrates were immersed in decyltrichlorosilane (DTS) solution (3 μL mL^{-1} in anhydrous toluene) at room temperature for 90 min to grow a hydrophobic self-assembled monolayer. Each polymer was dissolved in a mixture of 1,2-dichlorobenzene/chloroform (3:97, v/v) at a concentration of 10 mg mL^{-1} and then heated at 55 °C for 30 min. The substrate was placed on the center of the heating stage and held under vacuum via the chuck. Then, the upper shearing plate was lowered to contact the substrate. The polymer semiconductor thin films were deposited by the shearing method with optimized conditions, as previously reported.[59] The solution shearing deposition was performed under an ambient atmosphere at a substrate temperature of 25 °C and with a fixed moving speed of 1 mm s^{-1}, followed by postannealing at 55 °C under vacuum overnight. Finally, the 60 nm Au electrodes were deposited onto the polymer films under high vacuum through a shadow mask defining channels of 20 μm in length (L) and 1500 μm in width (W). The OFETs were completed with a bottom-gate top-contact (BGTC) architecture. The OFET characteristics were measured in the dark using a Keithley 4200 semiconductor analyzer under a N_2-filled atmosphere. The mobility (μ) was fitted by the data point of the transfer curve measured in the saturated region and calculated using eq 1:

$$I_d = \left(\frac{W}{2L}\right) C_i \mu \, (V_g - V_{th})^2 \quad (1)$$

where I_d is the drain current, C_i is the capacitance of the gate dielectric layer (~10 nF cm^{-2}), V_g is the gate voltage, and V_{th} is the threshold voltage.

The double transfer-printing technique was adopted to investigate the OFET properties of the stretched polymer films. The polymer films on the DTS-treated SiO_2/Si substrates were first transferred

https://doi.org/10.1021/acs.macromol.2c00957
Macromolecules 2022, 55, 10670−10681

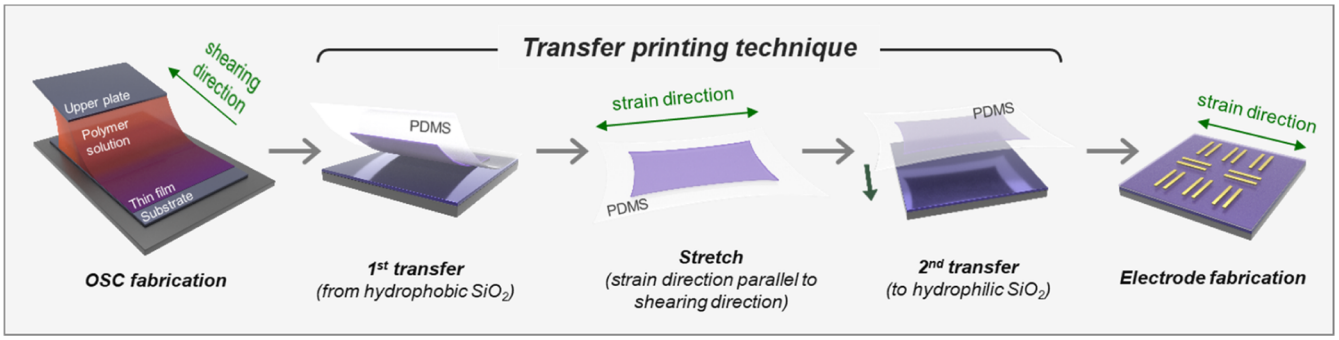

Figure 1. Schematic diagram of the process of stretched OFET devices.

Scheme 1. Synthesis of Diblock Copolymers PS_{85}–Zn–$P3HT_{187}$ (P1) and PS_{161}–Zn–$P3HT_{187}$ (P2)

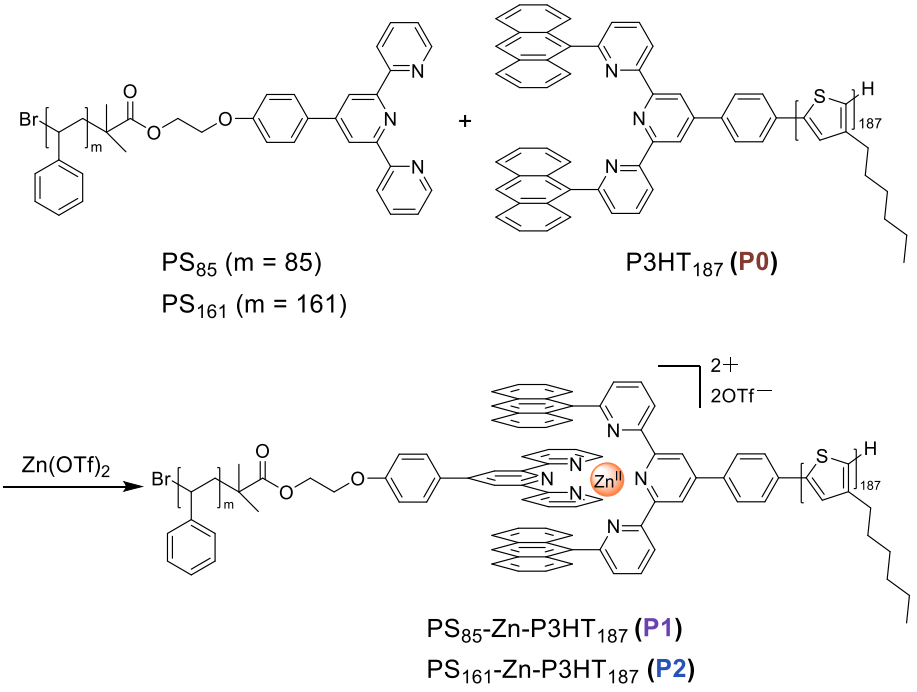

onto the poly(dimethylsiloxane) (PDMS) (base/crosslinker = 20:1 w/w) slabs and then stretched to strain values of 0, 25, 50, and 100%. Then, the stretched films were transferred to phenyltrichlorosilane-treated SiO_2/Si substrates. Finally, gold electrodes were deposited on the top to finish the OFET fabrication for further testing.

RESULTS AND DISCUSSION

Figure 1 shows the schematic illustration of the experimental method in this study. The solution shearing of the polymer semiconductors and the transfer printing process are used to fabricate the stretchable organic transistors with a uniaxially stretched structure in the elastomer template.

Polymer Synthesis. All the polymers were synthesized according to the previously reported procedures.[57,60] Generally, the well-defined tpy-modified PSs (PS_{85} and PS_{161}) were synthesized using an Fe(II)-bis(tpy) complex bearing an α-Bromoester as the metallo-initiator for the atom transfer radical polymerization of styrene. After decomplexation, the chain-end functionalized PSs with controllable molecular weights and low polydispersities ($Đ = M_w/M_n$) were realized. Under the optimized reaction conditions, two tpy-functionalized PS polymers with varying degrees of polymerization (DPs), namely, PS_{85} (M_n = 7900 Da, DP = 85, $Đ$ = 1.21) and PS_{161} (M_n = 16,200 Da, DP = 161, $Đ$ = 1.17), were obtained. Meanwhile, the well-defined $P3HT_{187}$ (**P0**, M_n = 36,500 Da, DP = 187, $Đ$ = 1.18) end-functionalized with a 6,6″-di(9-anthracenyl)-substituted tpy motif was obtained via the Suzuki–Miyaura coupling reaction of monobrominated P3HT with 6,6″-di(9-anthracenyl)-4′-(4-boronophenyl) tpy. Subsequently, the metallo-supramolecular diblock copolymers P1 and P2 were instantly constructed from PS_m (m = 85 or 161) and $P3HT_{187}$ upon complexation with $Zn(OTf)_2$ (Scheme 1). The chemical structures of copolymers **P1** and **P2** were unambiguously established by NMR spectroscopy (Figure S4). In particular, the characteristic shifts of the ^{1}H NMR signals after complexation strongly supported the quantitative formation of the heteroleptic Zn(II)-tpy complexes. Notably, the presence of the 9-anthracenyl substituents successfully avoided the formation of any unwanted homoleptic complexes.[57] As a result, the spontaneous heteroleptic complexation with Zn(II) ions led to the desired rod–coil block copolymers.

Polymer Characterization. The thermal behaviors of **P0**, **P1**, and **P2** were examined by differential scanning calorimetry (DSC) (Figure S6), and their thermal properties are summarized in Table 1. The thermogram of **P0** exhibits

https://doi.org/10.1021/acs.macromol.2c00957
Macromolecules 2022, 55, 10670−10681

Table 1. Thermal and Optical Properties and HOMO/LUMO Energy Levels of P0, P1, and P2

	T_c [°C][a]	T_m [°C][a]	ΔH_m [J g^{-1}][b]	λ_{max}^{soln} [nm]	λ_{0-0} [nm]	λ_{0-1} [nm]	A_{0-0}/A_{0-1}	$E_{g,opt}$ [eV][c]	E_{HOMO} [eV][d]	E_{LUMO} [eV][e]
P0	171.8	210.0	12.37	446	598	548	0.73	1.95	−4.78	−2.83
P1	158.3	204.9	7.57	446	594	544	0.70	1.96	−4.79	−2.83
P2	148.9	204.0	6.41	446	594	543	0.66	1.96	−4.75	−2.79

[a]The crystallization temperature (T_c) and melting temperature (T_m) were extracted from DSC scans. [b]The enthalpy of fusion was calculated from integrating the area under the second heating curves. [c]The optical energy band gap was extracted from the absorption band edge. [d]The HOMO levels were obtained by photoelectron spectroscopy in air (PESA). [e]The LUMO levels were calculated following the equation $E_{g,opt} = E_{HOMO} - E_{LUMO}$.

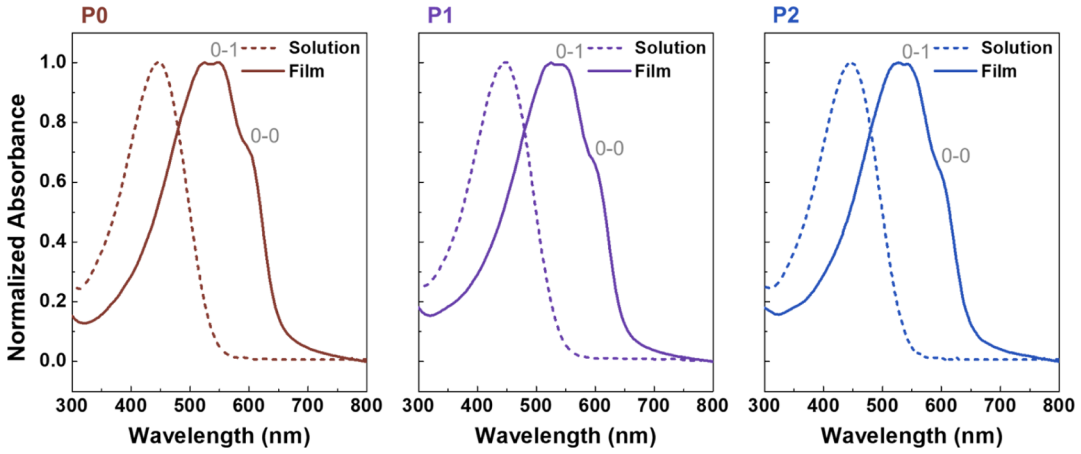

Figure 2. UV−vis spectra of **P0**, **P1**, and **P2** in solution (dashed line) and thin film (solid line).

pronounced endothermic and exothermic peaks that indicate a melting temperature (T_m) of 210.0 °C and a crystallization temperature (T_c) of 171.8 °C, which are consistent with those of typical P3HT homopolymers. For the block copolymers **P1** and **P2**, glass transition temperatures (T_g) of around 100 °C can be observed, corresponding to the segmental motion of the PS chains in the amorphous state. In addition, the block copolymers **P1** and **P2** exhibit P3HT melting peaks at around 204 °C (slightly lower than that of **P0**), along with crystallization temperatures of 158.3 and 148.9 °C, respectively. The lower T_m and T_c of the block copolymers relative to that of P3HT imply that the crystallization of P3HT is hindered by the PS chains.[48,61] Moreover, the enthalpy of fusion (ΔH_m) was calculated from the second heating curves to directly compare the crystallinity, and the corresponding ΔH_m values of the P3HT block in the copolymers were corrected according to the weight fraction of P3HT. The ΔH_m values of **P1** and **P2** were 10.03 and 10.66 J g^{-1}, respectively, whereas that of **P0** was 12.37 J g^{-1}. It has been reported that the perfect P3HT crystal shows a ΔH_m of 74 J g^{-1} derived from the Flory equation.[62] Thus, the relative crystallinities of P3HT in each polymer were determined to be 22.0, 13.6, and 14.4% for **P0**, **P1**, and **P2**, respectively.[48] The lower P3HT crystallinities of **P1** and **P2** relative to that of pristine P3HT (**P0**) indicate that the introduction of the coiled PS segment interferes with the packing behavior of P3HT. However, the P3HT crystallinity of **P2** is slightly higher than that of **P1**, thereby implying that the higher segregation strength between P3HT and the long PS chains in **P2** may generate a well-defined phase-separated domain in which the P3HT can be more orderly packed.[63]

The optical properties and polymer aggregation behavior of the block copolymers were characterized by UV−vis spectroscopy, and the normalized UV−vis spectra of the three polymers in the solution and thin film states are presented in Figure 2. The differences between the polymer interchain interaction strengths of the three polymers were determined by comparing the maximum absorption features associated with P3HT. In solution, the three polymers have similar absorption maxima at 452 nm due to the $\pi-\pi^*$ transition of the polythiophene main chain, thereby indicating that the incorporation of metal complexes and the formation of diblock copolymers with the PS segment have little impact on the polymer aggregation behavior. Meanwhile, the thin-film absorption spectrum of **P0** exhibits absorption maxima at 598 and 548 nm, corresponding to the 0−0 and 0−1 vibronic transitions, respectively, whereas **P1** and **P2** exhibit slightly blue-shifted absorption peaks, with a relatively lower 0−0 peak intensity. In detail, the absorption spectra of **P1** and **P2** exhibit peak maxima at 594 nm for the 0−0 transition, along with vibronic shoulders for the 0−1 transition at 544 and 543 nm, respectively. Moreover, the semiconducting molecular organization was quantitatively analyzed by calculating the ratio of the band intensities between the 0−0 and 0−1 vibronic peaks (A_{0-0}/A_{0-1}).[64] As this ratio is higher, it could be reasonably suggested that the polymers have better charge transport ability due to more ordered aggregates and the longer conjugation length of P3HT. As shown in Table 1, the ratio gradually decreases with the increase in PS block content, thus revealing the negative influence of the PS chains upon the aggregation behavior of P3HT, in agreement with the DSC data. All three polymers provide similar optical band gaps of ∼1.96 eV, as determined from the onsets of the thin-film absorption spectra. The highest occupied molecular orbital (HOMO) values were measured by photoelectron spectroscopy in air (PESA), as shown in Figure S7. Combined with these two values, the lowest unoccupied molecular orbital (LUMO) values were estimated, and the optical properties are

https://doi.org/10.1021/acs.macromol.2c00957
Macromolecules 2022, 55, 10670−10681

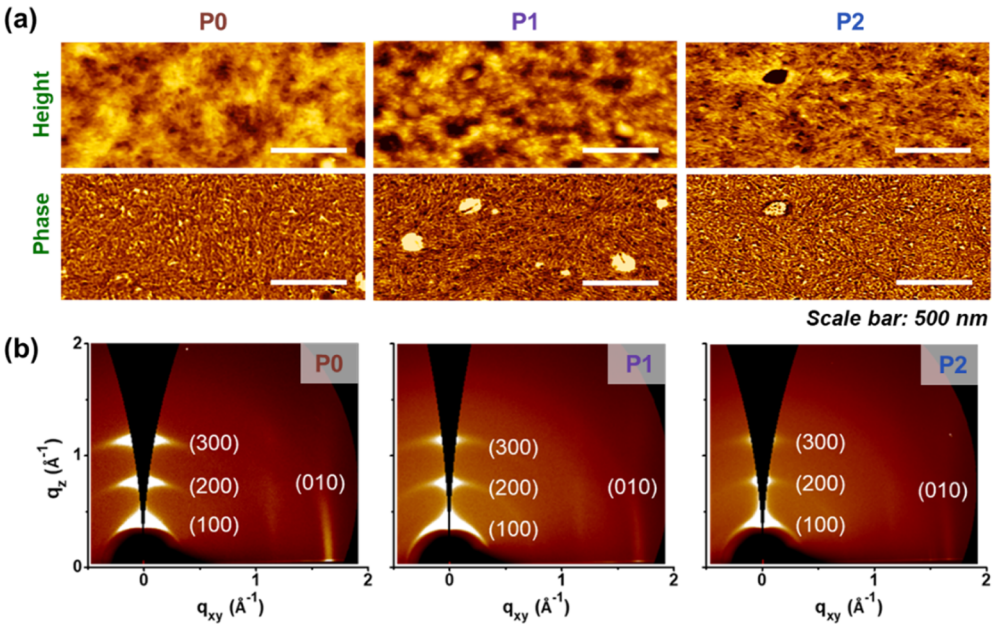

Figure 3. (a) AFM height (top) and phase (bottom) topographies of polymer thin films. (b) 2D-GIXRD patterns of polymer thin films (the shearing direction and the incident X-ray direction are parallel).

Table 2. Summary of the OFET Performance Results and the Relevant Crystallographic Parameters of the Three Polymer Films

	μ_{max} [cm^2 V^{-1} s^{-1}]	μ_{avg} [cm^2 V^{-1} s^{-1}]	I_{ON}/I_{OFF} [−]	V_{th} [V]	lamellar spacing [Å][a]	$\pi-\pi$ distance [Å]
P0	1.44×10^{-1}	$(8.14 \pm 3.19) \times 10^{-2}$	$10^3 \sim 10^6$	-15.9 ± 4.3	16.10	3.81
P1	8.86×10^{-2}	$(5.50 \pm 2.84) \times 10^{-2}$	$10^4 \sim 10^6$	-7.9 ± 1.9	16.10	3.79
P2	5.60×10^{-2}	$(5.07 \pm 1.34) \times 10^{-2}$	$10^3 \sim 10^5$	-2.8 ± 8.9	16.06	3.79

[a]Extracted from fitting the (100).

summarized in Table 1. Thus, all the energy levels of the three polymers are maintained at practically the same values, thereby indicating that the optical properties and electronic structures of the metallo-supramolecular block copolymers are similar and are mainly defined by the P3HT block.

Morphological Analysis of Polymer Thin Tilms

Atomic force microscopy (AFM) was conducted to examine the surface morphologies of the self-organized polymer films cast from a cosolvent of dichlorobenzene/chloroform (3:97 v/v). The height and phase images are presented in Figure 3a. Here, all the polymers clearly exhibit randomly oriented nanofibril structural characteristics with diameters of ∼15 nm, indicating similar P3HT-dominated aggregation behaviors in the copolymers. Such one-dimensional nanostructures have been shown to result from the strong $\pi-\pi$ interactions between the P3HT segments in the P3HT-based rod−coil block copolymers.[65,66] Although the UV−vis absorption spectra reveal a slightly lower degree of the ordered P3HT aggregate in the copolymers (Figure 2), they still tend to aggregate into nanofibrils that can facilitate charge transport. Thus, it can be inferred that the charge transport ability of the rod−coil block copolymers will not be seriously interrupted by the insulating PS segments. In addition, the root-mean-square roughness values in the AFM images of the **P0**, **P1**, and **P2** thin films are 3.24, 2.33, and 1.47 nm, respectively, thereby indicating that the flexible PS chains more efficiently fill the gaps between the P3HT nanofibrils to result in a smoother film surface. The 3D images of each AFM height image are provided in Figure S8 to ensure that the surface roughness is distinguishable from each other.

To gain more insights into the molecular packing of the polymer chains, two-dimensional synchrotron grazing incidence X-ray diffraction (2D-GIXRD) analysis was performed to identify the crystal structures. The 2D-GIXRD patterns in Figure 3b indicate that all three polymers exhibit well-defined third-order (h00) P3HT diffraction peaks in the out-of-plane direction (q_z), with lamellar spacings of 16.10 Å for **P0** and **P1** and 16.06 Å for **P2**. Furthermore, clear $\pi-\pi$ stacking peaks are observed for all the samples in the in-plane direction (q_{xy}), representing the predominant edge-on preferential arrangement on the surface. The corresponding $\pi-\pi$ stacking distances are 3.81 Å for **P0** and 3.79 Å for **P1** and **P2**. Based on the similar crystallographic parameters of the three polymers, it can be concluded that the P3HT chains in the copolymers pack in an identical manner to that of pure P3HT, that is, the alignment of the alkyl side chains and the $\pi-\pi$ stacking between neighboring thiophene rings are normal and parallel to the surface substrate, respectively. In other words, the introduction of the PS segment has little impact on the molecular orientation, so the charge transport channels of the conjugated P3HT domain can be preserved.

OFET Performances of Unstrained Polymer Films. To investigate the effect of the PS building block upon the charge transport abilities, top-contact/bottom-gate OFETs were fabricated via solution shearing of the polymer solution in a 3:97 volume ratio of 1,2-dichlorobenzene and chloroform onto the Si/SiO_2 substrates. On the top, 60 nm source and drain

https://doi.org/10.1021/acs.macromol.2c00957
Macromolecules 2022, 55, 10670−10681

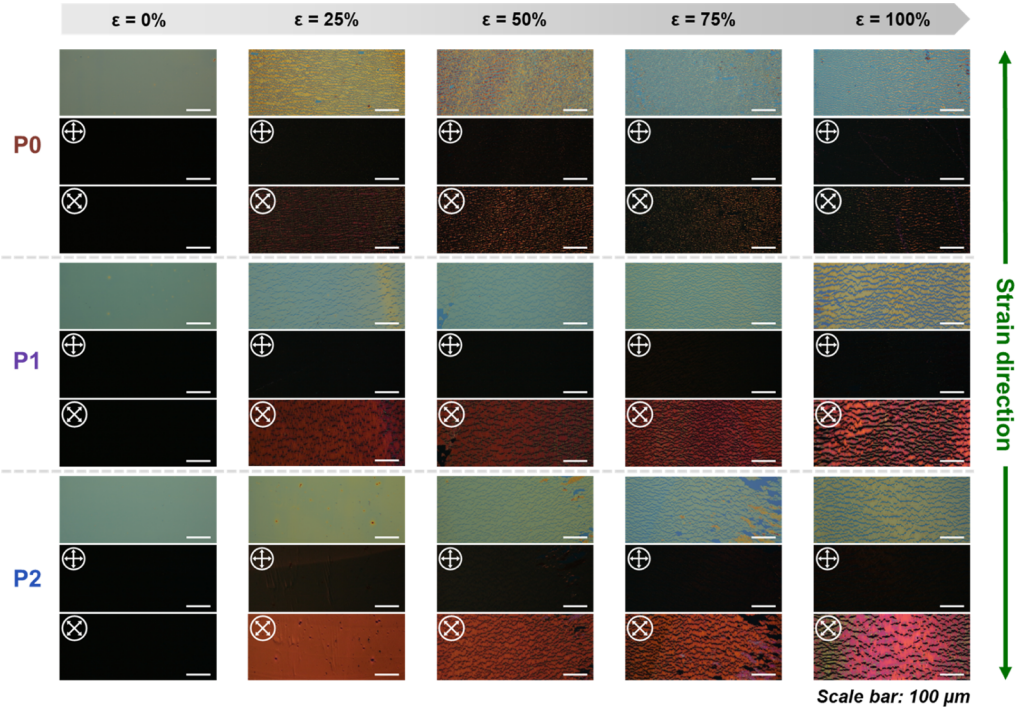

Figure 4. OM images (top) and POM images of the **P0**, **P1**, and **P2** thin films at orientations of 0° (middle) and 45° (bottom) to the polarization of the incident light.

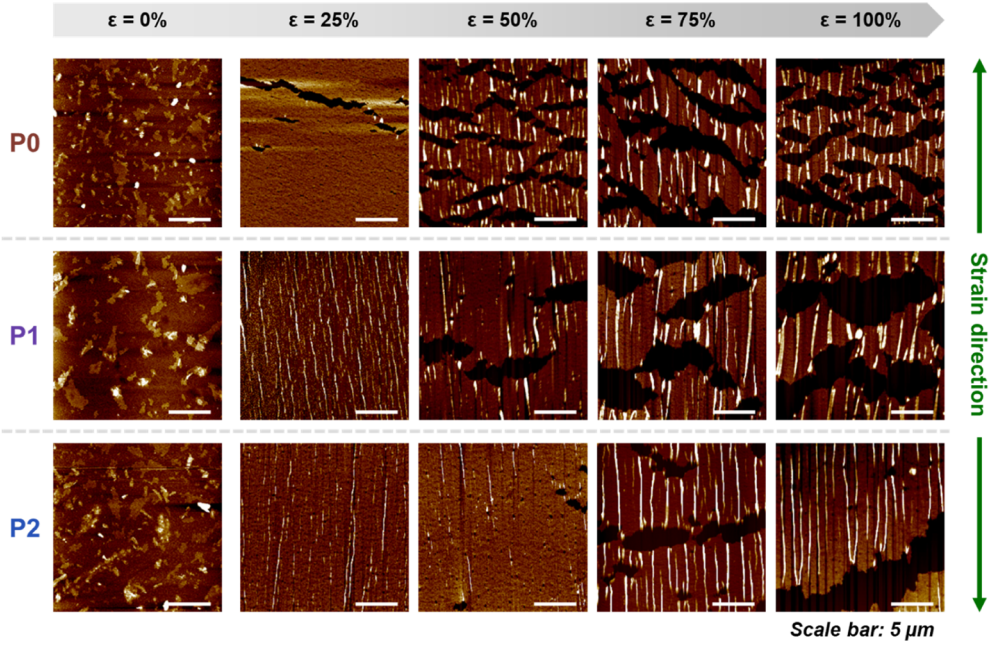

Figure 5. AFM images of the **P0**, **P1**, and **P2** films under 0, 25, 50, 75, and 100% strain.

gold electrodes were thermally evaporated to finish the device. The transfer and output characteristics are shown in Figure S9, and all the OFET characteristic parameters, including the μ, the ON/OFF ratio (I_{ON}/I_{OFF}), and the threshold voltage (V_{th}), are summarized in Table 2. Since the anisotropy due to the solution process is of little importance compared to the effect of stretching, it is discussed in the following section. In the present section, the μ is examined with the charge transport direction parallel to the shearing direction. Here, **P0** exhibits an average mobility (μ_{avg}) of $(8.14 \pm 3.19) \times 10^{-2}$ cm^2 V^{-1} s^{-1}, while **P1** and **P2** exhibit slightly lower μ_{avg} values of $(5.50 \pm 2.84) \times 10^{-2}$ and $(5.07 \pm 1.34) \times 10^{-2}$ cm^2 V^{-1} s^{-1}, respectively. These mobilities are comparable with those of other reported polythiophene-based homopolymers or block copolymers.[49−51,67] According to the abovementioned AFM analysis, the P3HT domains in **P1** and **P2** have the same nanofibrillar form as that of **P0**, and thus, **P1** and **P2** maintain similar charge transport abilities to that of **P0**. The slight reduction in the mobilities of **P1** and **P2** can be attributed to the insulating PS domains embedded within the polymer thin

https://doi.org/10.1021/acs.macromol.2c00957
Macromolecules 2022, 55, 10670−10681

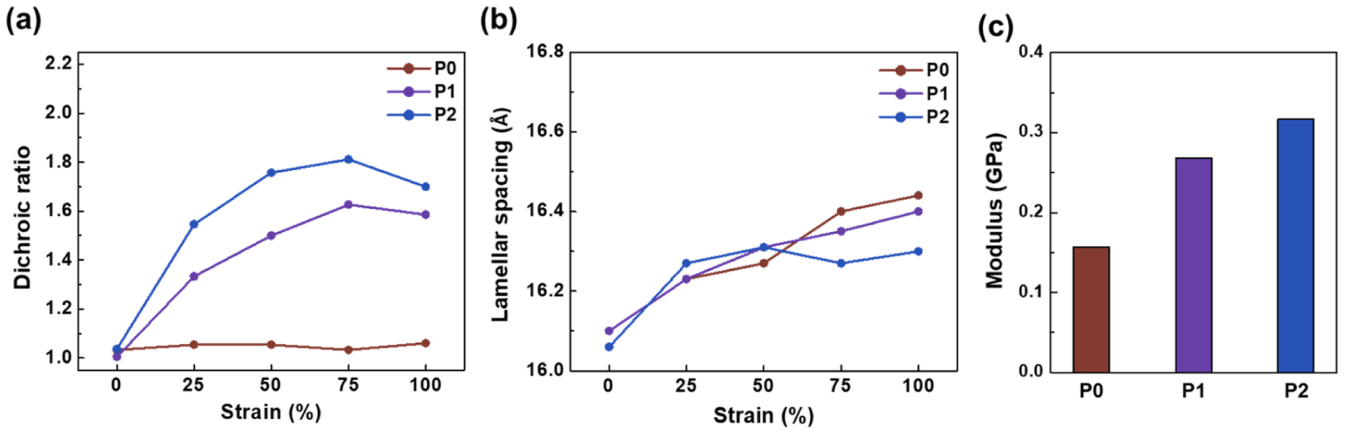

Figure 6. (a) DR and (b) (100) lamellar spacing under strain. (c) Elastic moduli of the three polymer films.

films. In addition, based on the DSC analysis, the P3HT blocks of **P1** and **P2** have slightly lower crystallinities, which also cause the charge mobilities to decrease. The devices exhibit identical I_{ON}/I_{OFF} values in the range of 10^3-10^6. The V_{th} of **P0** is slightly higher than that of **P1** and **P2**, thereby suggesting the possible presence of some defects resulting from the end-chain functionalized 6,6″-di(9-anthracenyl)-substituted tpy motifs in the copolymers.

Structure–Stretchability Relationship of Polymer Films. After stretching, the fractures in the films were directly observed via optical microscopy (OM). For the stretching test, the films were transferred onto PDMS slabs from the silane-modified Si/SiO_2 substrates on which they were initially cast, as described in the previous report.[68] The films were then stretched on the PDMS elastomer at a specific strain (ε) and then transferred back to the substrate for visual inspection by OM. It should be noted that the stretching direction is the same as the shearing direction for all characterizations under stretching. In Figure 4, the **P0** and **P1** films exhibit tearing features at onset strains of 25%, whereas there is no evident cracking of **P2** under the same stretching condition, suggesting that the block copolymers with a longer random coil PS chain can endure a larger strain. In addition to OM, AFM was used to observe the microscale morphologies of the stretched films, and the influence of strain upon the polymer films is more clearly revealed by the height images in Figure 5. Here, the stretching conditions are similar to those observed in the OM images. For the **P0** thin film with only rigid P3HT chains, the low entanglements and few tie chains between the P3HT crystallites result in low ductility, and cracks appear under the low strain of 25%. At higher strains of 25–100%, wrinkles along the stretching direction, combined with slightly larger cracks, are clearly observed. For the case of the ductile **P2** film, wrinkles are produced at the low strain of 25%, and isolated microvoids are initiated at 75% strain, and propagated with the increased strain. Furthermore, the polymer backbones are seen to be oriented according to the applied strain, as can be observed in the polarized optical microscopy (POM) images in Figure 4. Here, **P1** and **P2** exhibit pronounced birefringence when the crossed polarizer and analyzer are placed at 45° with respect to the stretching direction, and this birefringence becomes stronger as the strain is increased, especially for the **P2** film. By contrast, the POM images at 45° for **P0** only exhibit weak birefringence, even at large strains. These observations suggest that **P1** and **P2** are better oriented than **P0** upon stretching. In the POM images at 0°, all of the films are dark, further indicating that the polymer chains are aligned with the stretching.

The variation in the backbone alignment of the three polymers with respect to the strain direction can be compared by calculating the dichroic ratio (DR) with applied strain from the UV–vis spectra under linearly polarized illumination (Figure S10). The DR is defined as $A_{//}/A_{\perp}$, where A is the maximum absorbance of the films with the polarized light parallel (//) and perpendicular ($\perp$) to the applied strain direction. In Figure 6a, the DR values of the **P1** and **P2** films are seen to be linearly increased upon stretching, thereby revealing that the block copolymers with amorphous PS segments can endure higher strain levels and tend to retain their aligned chains under plastic deformation,[17] rather than fracturing to release the stress. Further, **P2** with its long PS chains exhibits the highest DR, whereas that of **P0** is little changed with a value of ~1 during stretching, that is, isotropic absorbance occurs without orientation, consistent with the abovementioned OM observations. However, the DR values of the copolymers **P1** and **P2** are found to decrease slightly at 100% strain, thereby suggesting an upper limit to their strain tolerance.

The 2D-GIXRD analyses were also conducted to investigate the variations in the crystalline microstructures of the thin films under strain. The change in the lamellar spacings was extracted from the original 2D diffraction patterns (Figures S11 and S12) and are summarized in Figure 6b. The relevant crystallographic parameters are summarized in Table S1. Upon strain, the lamellar spacings gradually increase due to the displacement of the P3HT stacking layers. In addition, quantitative nanomechanical mapping was used to determine the elastic moduli by applying the Derjaguin–Muller–Toporov (DMT) contact mechanics model in order to clearly evaluate the mechanical properties of the polymer thin films. A histogram of the moduli measured over 128 × 128 pixels covering the area of 1 × 1 μm^2 is presented in Figure S13. As indicated in Figure 6c, the elastic moduli of **P0**, **P1**, and **P2** are 0.157, 0.268, and 0.317 GPa, respectively. According to the previous report,[69] the elastic modulus of P3HT is about 0.2 GPa, which is lower than that of PS (the latter being usually a few gigapascals). It is therefore reasonable to find that the moduli of **P1** and **P2** are higher than that of **P0**. Nevertheless, **P1** and **P2** have better deformability and stretchability because the introduction of the flexible PS chains gives rise to amorphous PS domains that can act as strain energy-

https://doi.org/10.1021/acs.macromol.2c00957
Macromolecules 2022, 55, 10670–10681

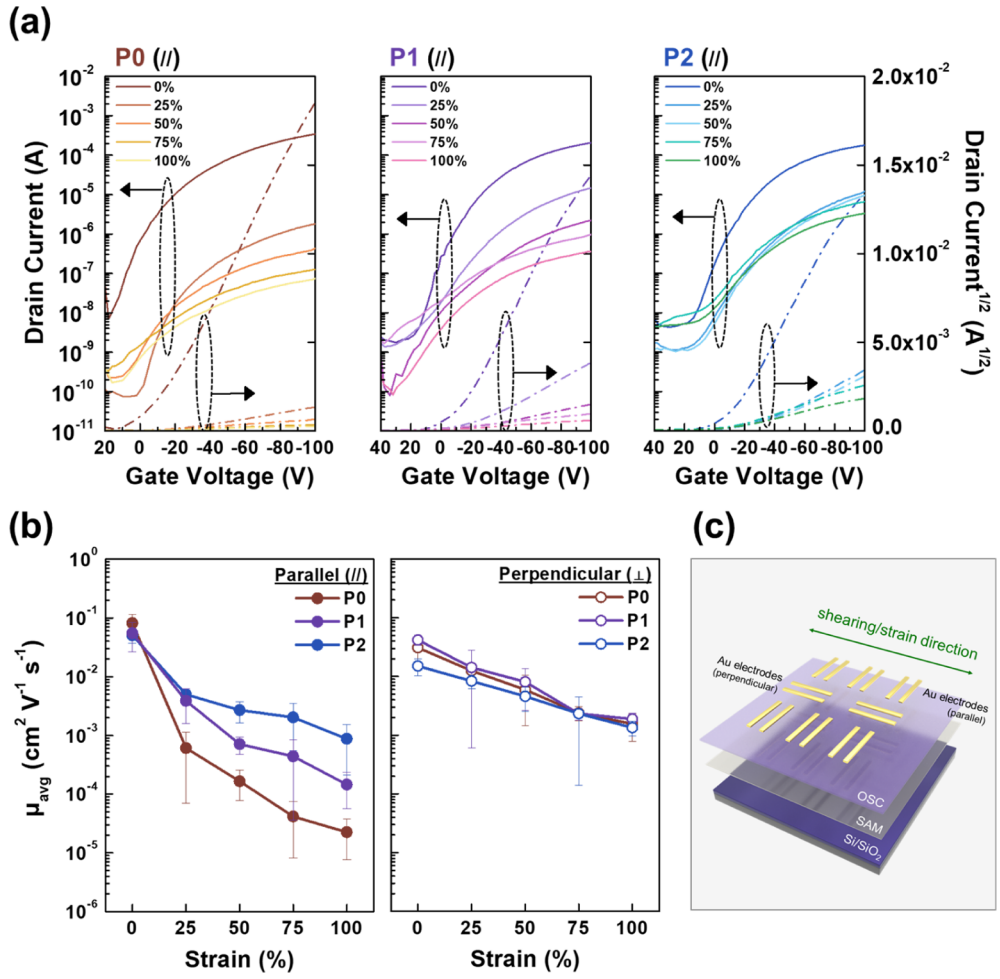

Figure 7. (a) Transfer curves of the OFETs based on the **P0**, **P1**, and **P2** thin films under strain direction. (b) Change in mobilities of the stretched OFETs under strains parallel and perpendicular to the charge transport direction. (c) Schematic illustration of the BGTC OFET device structure, showing the strain direction with respect to the charge transport channel.

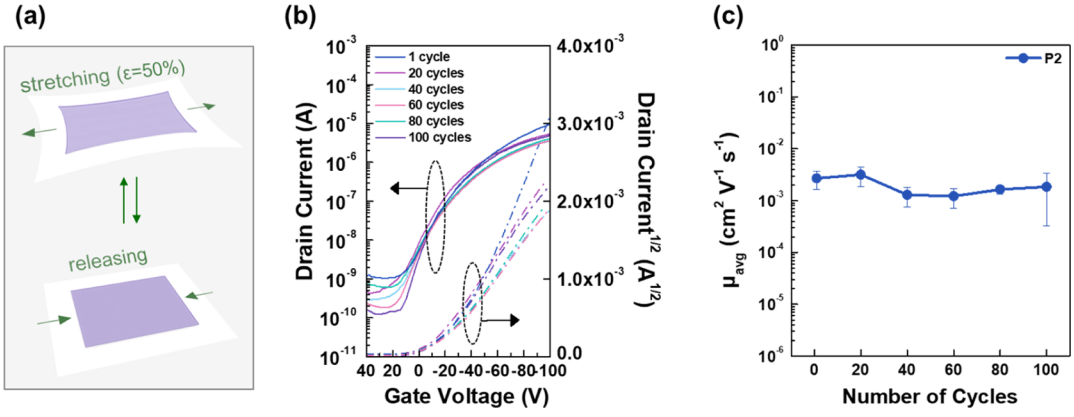

Figure 8. (a) Schematic diagram of the repeated stretching/releasing test under 50% strain. (b) Transfer curves (c) change in mobility of **P2** after repeated stretching/releasing for 1, 20, 40, 60, 80, and 100 cycle (s) under strain parallel to the charge transport direction.

dissipating regions and prevent the P3HT from becoming damaged under stretching.

OFET Characteristics of Stretched Polymer Films. The electrical properties of the OFETs based on the homopolymer **P0** and block copolymers **P1** and **P2** under applied strains parallel and perpendicular to the channel direction were also investigated. The transfer curves under various parallel strains of 25, 50, 75, and 100% are presented in Figure 7a, the μ under parallel (//) and perpendicular (⊥) strains are plotted in Figure 7b, and the structure of the stretched device is shown schematically in Figure 7c. The complete OFET parameters in both directions are summarized in Tables S2 and S3. Obviously, as the strain is increased from 0 to 25% parallel to the charge transport direction, the ON state current of **P0** considerably decreases compared to that of the other two samples (Figure 7a), which indicates the deformation of the

https://doi.org/10.1021/acs.macromol.2c00957
Macromolecules 2022, 55, 10670−10681

block copolymer films under the high stretching. With the increase in strain from 25 to 100%, the calculated maximum mobility (μ_{max}) of **P2** (//) decreases from 5.48×10^{-3} to 1.40×10^{-3} cm^2 V^{-1} s^{-1} and that of **P0** (//) decreases from 8.32×10^{-4} to 3.13×10^{-5} cm^2 V^{-1} s^{-1}. Here, the mechanical cracking of the **P0** film starting at 25% stretching contributes to the significantly diminished electrical properties by greatly obstructing the charge transport pathway in the direction parallel to the strain. This observed change in μ under parallel strain can account for the high strain tolerance of the block copolymer films due to the amorphous sites of the additional PS segment and the stretching-induced **P2** backbone alignment. By contrast, the cracks formed in the **P0** film have less impact on the μ when the stretching is applied in the perpendicular direction. Indeed, the μ under strain in the perpendicular direction is seen to increase slightly more than that in the parallel direction for all samples, probably because the cracks are oriented across the channels. In other words, because the cracks are perpendicular to the channel, the perpendicular strain provides a remaining partial charge transport channel.

To further demonstrate the stretching stability, the most stretchable of all the polymers studied herein, namely, **P2**, was subjected to a cyclic stretching−releasing test. In this procedure, the **P2**/PDMS film stack was repeatedly strained to 50% and then released back to its initial unstrained state, as shown schematically in Figure 8a. After the cyclic strain process was complete, the film was characterized while transfer printed onto the secondary silane-modified substrate. The OFET properties of the **P2** (//) sample after various numbers of cycles (1−100) are indicated in Figure 8b and Table S4, and the corresponding changes in mobility are plotted in Figure 8c. Here, the mobility is seen to be retained at a certain level, even after stretching and releasing for 100 times, thereby demonstrating the excellent tolerance and potential of this polymer for application in wearable electronics.

Based on the above results and discussion, the details of the metallo-supramolecular rod−coil block copolymers for stretchability and charge transport properties were systematically studied. It can be inferred that the additional PS block can effectively enhance the deformability of the semiconducting polymer because the amorphous coil chains can support the external strain and delay or limit crack onset. Their amorphous nature can allow for greater strain due to the large volume available for chain movement, and the charge transport is not significantly disrupted even by the introduction of the random coil disorder. We believe that the dynamic metal−ligand coordination bonds introduced for linkage between the rod and coil blocks can assist the chain alignment under stress, significantly enhance the stretchability in terms of a high modulus, increase the content of the amorphous domain, and maintain moderate-to-high mobility via interchain hopping charge transport.

On the other hand, tests on the blended systems were also performed to compare with the block copolymers in this study. For the blending system, P3HT and tpy-modified PS were used, and the effect of amorphous PS without Zn complexation can be discussed. Detailed characterizations are included in the fifth section of the Supporting Information and Figures S22−S25. These results provide evidence that the blending strategy is unsuitable for stretchable OFET applications based on the transferring technique and that the block copolymer is a better solution.

CONCLUSIONS

We explored the feasibility of a series of metallo-supramolecular rod−coil block copolymers for stretchable OFETs, where the block copolymers contain crystalline P3HT segments connected to amorphous PS segments via metal−ligand coordination. The as-proposed one-pot self-assembly strategy can be readily applied to the construction of various stretchable polymer semiconductors. The addition of the PS block into the block copolymers was shown to increase the film stretchability while maintaining the charge transport ability. The chain entanglement from amorphous PS provided the primary resistance against deformation, thereby helping sustain the charge mobility under strain. The strain-oriented block copolymer **P2** retained a mobility of 1.40×10^{-3} cm^2 V^{-1} s^{-1} under 100% strain, which was approximately 100 times greater than that of the homopolymer counterpart **P0**. This large increase in stretchability in the proof-of-concept metallo-supramolecular block copolymers demonstrates a viable approach toward mechanically robust and wearable organic electronic devices. In future, the metallo-supramolecular copolymers based on semicrystalline P3HT will be designed and synthesized with specific amorphous and ductile polymer blocks for a reduced T_g in order to meet the requisite morphologies for mechanical compliance and, thus, expand the novel molecular design of stretchable polymer semiconductors.

ASSOCIATED CONTENT

Supporting Information

The Supporting Information is available free of charge at https://pubs.acs.org/doi/10.1021/acs.macromol.2c00957.

Materials and measurements, synthesis of polymers, ^{1}H-NMR spectra, DSC thermograms, PESA measurements, transfer and output plots, 2D-GIXRD patterns, DMT modulus mappings and histograms, and results and discussion of PS/P3HT blending tests (PDF).

AUTHOR INFORMATION

Corresponding Authors

Yi-Tsu Chan − *Department of Chemistry, National Taiwan University, Taipei 10617, Taiwan;* orcid.org/0000-0001-9658-2188; Email: ytchan@ntu.edu.tw

Cheng-Liang Liu − *Department of Materials Science and Engineering, National Taiwan University, Taipei 10617, Taiwan;* orcid.org/0000-0002-8778-5386; Email: liucl@ntu.edu.tw

Authors

Wei-Ni Wu − *Department of Materials Science and Engineering, National Taiwan University, Taipei 10617, Taiwan*

Tsung-Han Tu − *Department of Chemistry, National Taiwan University, Taipei 10617, Taiwan*

Chiao-Hsuan Pai − *Department of Chemistry, National Taiwan University, Taipei 10617, Taiwan*

Kuan-Heng Cheng − *Department of Chemistry, National Taiwan University, Taipei 10617, Taiwan*

Shih-Huang Tung − *Institute of Polymer Science and Engineering, National Taiwan University, Taipei 10617, Taiwan;* orcid.org/0000-0002-6787-4955

Complete contact information is available at: https://pubs.acs.org/10.1021/acs.macromol.2c00957

Notes

The authors declare no competing financial interest.

■ ACKNOWLEDGMENTS

Y.-T.C. thanks the financial support from the Ministry of Science and Technology (MOST) of Taiwan (109-2113-M-002-019-MY3 and 110-2113-M-001-062) and the Center for Emerging Materials and Advanced Devices at National Taiwan University (NTU110L880504). C.-L.L. gratefully acknowledges the Young Scholar Fellowship Program (Columbus Program) and 2030 Cross-Generation Young Scholars Program by MOST in Taiwan, under grants 110-2636-E-002-021 and 111-2628-E-002-014, respectively. The authors thank Beamline B13A1/B17A1/B23A1 from the National Synchrotron Radiation Research Center (NSRRC) of Taiwan for providing beamtime. This article was subsidized for English editing by National Taiwan University under the Excellence Improvement Program for Doctoral Students (grant number 108-2926-I-002-002-MY4), sponsored by MOST, Taiwan.

■ REFERENCES

(1) Root, S. E.; Savagatrup, S.; Printz, A. D.; Rodriquez, D.; Lipomi, D. J. Mechanical Properties of Organic Semiconductors for Stretchable, Highly Flexible, and Mechanically Robust Electronics. *Chem. Rev.* **2017**, *117*, 6467−6499.

(2) Trung, T. Q.; Lee, N.-E. Recent Progress on Stretchable Electronic Devices with Intrinsically Stretchable Components. *Adv. Mater.* **2017**, *29*, 1603167.

(3) Kleinschmidt, A. T.; Lipomi, D. J. Stretchable Conjugated Polymers: A Case Study in Topic Selection for New Research Groups. *Acc. Chem. Res.* **2018**, *51*, 3134−3143.

(4) Sim, K.; Rao, Z.; Ershad, F.; Yu, C. Rubbery Electronics Fully Made of Stretchable Elastomeric Electronic Materials. *Adv. Mater.* **2020**, *32*, 1902417.

(5) Wang, X.; Liu, Y.; Chen, Q.; Yan, Y.; Rao, Z.; Lin, Z.; Chen, H.; Guo, T. Recent Advances in Stretchable Field-Effect Transistors. *J. Mater. Chem. C* **2021**, *9*, 7796−7828.

(6) Savagatrup, S.; Printz, A. D.; O'Connor, T. F.; Zaretski, A. V.; Lipomi, D. J. Molecularly Stretchable Electronics. *Chem. Mater.* **2014**, *26*, 3028−3041.

(7) Lee, Y.; Shin, M.; Thiyagarajan, K.; Jeong, U. Approaches to Stretchable Polymer Active Channels for Deformable Transistors. *Macromolecules* **2016**, *49*, 433−444.

(8) Qian, Y.; Zhang, X.; Xie, L.; Qi, D.; Chandran, B. K.; Chen, X.; Huang, W. Stretchable Organic Semiconductor Devices. *Adv. Mater.* **2016**, *28*, 9243−9265.

(9) Ashizawa, M.; Zheng, Y.; Tran, H.; Bao, Z. Intrinsically Stretchable Conjugated Polymer Semiconductors in Field Effect Transistors. *Prog. Polym. Sci.* **2020**, *100*, 101181.

(10) Zheng, Y.; Zhang, S.; Tok, J. B. H.; Bao, Z. Molecular Design of Stretchable Polymer Semiconductors: Current Progress and Future Directions. *J. Am. Chem. Soc.* **2022**, *144*, 4699−4715.

(11) Tien, H.-C.; Huang, Y.-W.; Chiu, Y.-C.; Cheng, Y.-H.; Chueh, C.-C.; Lee, W.-Y. Intrinsically Stretchable Polymer Semiconductors: Molecular Design, Processing and Device Applications. *J. Mater. Chem. C* **2021**, *9*, 2660−2684.

(12) Ocheje, M. U.; Charron, B. P.; Nyayachavadi, A.; Rondeau-Gagné, S. Stretchable Electronics: Recent Progress in the Preparation of Stretchable and Self-Healing Semiconducting Conjugated Polymers. *Flexible Printed Electron.* **2017**, *2*, 043002.

(13) Wang, G.-J. N.; Gasperini, A.; Bao, Z. Stretchable Polymer Semiconductors for Plastic Electronics. *Adv. Electron. Mater.* **2018**, *4*, 1700429.

(14) Wang, M.; Baek, P.; Akbarinejad, A.; Barker, D.; Travas-Sejdic, J. Conjugated Polymers and Composites for Stretchable Organic Electronics. *J. Mater. Chem. C* **2019**, *7*, 5534−5552.

(15) Janasz, L.; Borkowski, M.; Blom, P. W. M.; Marszalek, T.; Pisula, W. Organic Semiconductor/Insulator Blends for Elastic Field-Effect Transistors and Sensors. *Adv. Funct. Mater.* **2022**, *32*, 2105456.

(16) Ding, Z.; Liu, D.; Zhao, K.; Han, Y. Optimizing Morphology to Trade Off Charge Transport and Mechanical Properties of Stretchable Conjugated Polymer Films. *Macromolecules* **2021**, *54*, 3907−3926.

(17) Oh, J. Y.; Rondeau-Gagné, S.; Chiu, Y.-C.; Chortos, A.; Lissel, F.; Wang, G.-J. N.; Schroeder, B. C.; Kurosawa, T.; Lopez, J.; Katsumata, T.; Xu, J.; Zhu, C.; Gu, X.; Bae, W.-G.; Kim, Y.; Jin, L.; Chung, J. W.; Tok, J. B. H.; Bao, Z. Intrinsically Stretchable and Healable Semiconducting Polymer for Organic Transistors. *Nature* **2016**, *539*, 411−415.

(18) Mun, J.; Wang, G.-J. N.; Oh, J. Y.; Katsumata, T.; Lee, F. L.; Kang, J.; Wu, H.-C.; Lissel, F.; Rondeau-Gagné, S.; Tok, J. B. H.; Bao, Z. Effect of Nonconjugated Spacers on Mechanical Properties of Semiconducting Polymers for Stretchable Transistors. *Adv. Funct. Mater.* **2018**, *28*, 1804222.

(19) Oh, J. Y.; Son, D.; Katsumata, T.; Lee, Y.; Kim, Y.; Lopez, J.; Wu, H.-C.; Kang, J.; Park, J.; Gu, X.; Mun, J.; Wang, N. G.-J.; Yin, Y.; Cai, W.; Yun, Y.; Tok, J. B. H.; Bao, Z. Stretchable Self-Healable Semiconducting Polymer Film for Active-Matrix Strain-Sensing Array. *Sci. Adv.* **2019**, *5*, No. eaav3097.

(20) Zheng, Y.; Ashizawa, M.; Zhang, S.; Kang, J.; Nikzad, S.; Yu, Z.; Ochiai, Y.; Wu, H.-C.; Tran, H.; Mun, J.; Zheng, Y.-Q.; Tok, J. B. H.; Gu, X.; Bao, Z. Tuning the Mechanical Properties of a Polymer Semiconductor by Modulating Hydrogen Bonding Interactions. *Chem. Mater.* **2020**, *32*, 5700−5714.

(21) Wu, H.-C.; Lissel, F.; Wang, G.-J. N.; Koshy, D. M.; Nikzad, S.; Yan, H.; Xu, J.; Luo, S.; Matsuhisa, N.; Cheng, Y.; Wang, F.; Ji, B.; Li, D.; Chen, W.-C.; Xue, G.; Bao, Z. Metal−Ligand Based Mechanophores Enhance Both Mechanical Robustness and Electronic Performance of Polymer Semiconductors. *Adv. Funct. Mater.* **2021**, *31*, 2009201.

(22) Li, Y.; Tatum, W. K.; Onorato, J. W.; Zhang, Y.; Luscombe, C. K. Low Elastic Modulus and High Charge Mobility of Low-Crystallinity Indacenodithiophene-Based Semiconducting Polymers for Potential Applications in Stretchable Electronics. *Macromolecules* **2018**, *51*, 6352−6358.

(23) Zheng, Y.; Wang, G.-J. N.; Kang, J.; Nikolka, M.; Wu, H.-C.; Tran, H.; Zhang, S.; Yan, H.; Chen, H.; Yuen, P. Y.; Mun, J.; Dauskardt, R. H.; McCulloch, I.; Tok, J. B. H.; Gu, X.; Bao, Z. An Intrinsically Stretchable High-Performance Polymer Semiconductor with Low Crystallinity. *Adv. Funct. Mater.* **2019**, *29*, 1905340.

(24) Wu, H.-C.; Hung, C.-C.; Hong, C.-W.; Sun, H.-S.; Wang, J.-T.; Yamashita, G.; Higashihara, T.; Chen, W.-C. Isoindigo-Based Semiconducting Polymers Using Carbosilane Side Chains for High Performance Stretchable Field-Effect Transistors. *Macromolecules* **2016**, *49*, 8540−8548.

(25) Chiang, Y.-C.; Wu, H.-C.; Wen, H.-F.; Hung, C.-C.; Hong, C.-W.; Kuo, C.-C.; Higashihara, T.; Chen, W.-C. Tailoring Carbosilane Side Chains toward Intrinsically Stretchable Semiconducting Polymers. *Macromolecules* **2019**, *52*, 4396−4404.

(26) Huang, Y.-W.; Lin, Y.-C.; Yen, H.-C.; Chen, C.-K.; Lee, W.-Y.; Chen, W.-C.; Chueh, C.-C. High Mobility Preservation of near Amorphous Conjugated Polymers in the Stretched States Enabled by Biaxially-Extended Conjugated Side-Chain Design. *Chem. Mater.* **2020**, *32*, 7370−7382.

(27) Lin, Y.-C.; Chen, F.-H.; Chiang, Y.-C.; Chueh, C.-C.; Chen, W.-C. Asymmetric Side-Chain Engineering of Isoindigo-Based Polymers for Improved Stretchability and Applications in Field-Effect Transistors. *ACS Appl. Mater. Interfaces* **2019**, *11*, 34158−34170.

(28) Yen, H.-C.; Lin, Y.-C.; Chen, W.-C. Modulation of the Hydrophilicity on Asymmetric Side Chains of Isoindigo-Based Polymers for Improving Carrier Mobility−Stretchability Properties. *Macromolecules* **2021**, *54*, 1665−1676.

(29) Wen, H.-F.; Wu, H.-C.; Aimi, J.; Hung, C.-C.; Chiang, Y.-C.; Kuo, C.-C.; Chen, W.-C. Soft Poly(Butyl Acrylate) Side Chains

https://doi.org/10.1021/acs.macromol.2c00957
Macromolecules 2022, 55, 10670−10681

toward Intrinsically Stretchable Polymeric Semiconductors for Field-Effect Transistor Applications. *Macromolecules* **2017**, *50*, 4982−4992.
(30) Lin, Y.-C.; Shih, C.-C.; Chiang, Y.-C.; Chen, C.-K.; Chen, W.-C. Intrinsically Stretchable Isoindigo−Bithiophene Conjugated Copolymers Using Poly(Acrylate Amide) Side Chains for Organic Field-Effect Transistors. *Polym. Chem.* **2019**, *10*, 5172−5183.
(31) Lin, Y.-C.; Chen, C.-K.; Chiang, Y.-C.; Hung, C.-C.; Fu, M.-C.; Inagaki, S.; Chueh, C.-C.; Higashihara, T.; Chen, W.-C. Study on Intrinsic Stretchability of Diketopyrrolopyrrole-Based Π-Conjugated Copolymers with Poly(Acryl Amide) Side Chains for Organic Field-Effect Transistors. *ACS Appl. Mater. Interfaces* **2020**, *12*, 33014−33027.
(32) Choi, D.; Kim, H.; Persson, N.; Chu, P.-H.; Chang, M.; Kang, J.-H.; Graham, S.; Reichmanis, E. Elastomer−Polymer Semiconductor Blends for High-Performance Stretchable Charge Transport Networks. *Chem. Mater.* **2016**, *28*, 1196−1204.
(33) Xu, J.; Wang, S.; Wang, G.-J. N.; Zhu, C.; Luo, S.; Jin, L.; Gu, X.; Chen, S.; Feig, V. R.; To, J. W. F.; Rondeau-Gagné, S.; Park, J.; Schroeder, B. C.; Lu, C.; Oh, J. Y.; Wang, Y.; Kim, Y.-H.; Yan, H.; Sinclair, R.; Zhou, D.; Xue, G.; Murmann, B.; Linder, C.; Cai, W.; Tok, J. B. H.; Chung, J. W.; Bao, Z. Highly Stretchable Polymer Semiconductor Films through the Nanoconfinement Effect. *Science* **2017**, *355*, 59.
(34) Zhang, G.; McBride, M.; Persson, N.; Lee, S.; Dunn, T. J.; Toney, M. F.; Yuan, Z.; Kwon, Y.-H.; Chu, P.-H.; Risteen, B.; Reichmanis, E. Versatile Interpenetrating Polymer Network Approach to Robust Stretchable Electronic Devices. *Chem. Mater.* **2017**, *29*, 7645−7652.
(35) Tran, H.; Feig, V. R.; Liu, K.; Wu, H.-C.; Chen, R.; Xu, J.; Deisseroth, K.; Bao, Z. Stretchable and Fully Degradable Semiconductors for Transient Electronics. *ACS Cent. Sci.* **2019**, *5*, 1884−1891.
(36) Xu, J.; Wu, H.-C.; Zhu, C.; Ehrlich, A.; Shaw, L.; Nikolka, M.; Wang, S.; Molina-Lopez, F.; Gu, X.; Luo, S.; Zhou, D.; Kim, Y.-H.; Wang, G.-J. N.; Gu, K.; Feig, V. R.; Chen, S.; Kim, Y.; Katsumata, T.; Zheng, Y.-Q.; Yan, H.; Chung, J. W.; Lopez, J.; Murmann, B.; Bao, Z. Multi-Scale Ordering in Highly Stretchable Polymer Semiconducting Films. *Nat. Mater.* **2019**, *18*, 594−601.
(37) Zhang, S.; Cheng, Y.-H.; Galuska, L.; Roy, A.; Lorenz, M.; Chen, B.; Luo, S.; Li, Y.-T.; Hung, C.-C.; Qian, Z.; St. Onge, P. B. J.; Mason, G. T.; Cowen, L.; Zhou, D.; Nazarenko, S. I.; Storey, R. F.; Schroeder, B. C.; Rondeau-Gagné, S.; Chiu, Y.-C.; Gu, X. Tacky Elastomers to Enable Tear-Resistant and Autonomous Self-Healing Semiconductor Composites. *Adv. Funct. Mater.* **2020**, *30*, 2000663.
(38) Klok, H. A.; Lecommandoux, S. Supramolecular Materials Via Block Copolymer Self-Assembly. *Adv. Mater.* **2001**, *13*, 1217−1229.
(39) Mai, Y.; Eisenberg, A. Self-Assembly of Block Copolymers. *Chem. Soc. Rev.* **2012**, *41*, 5969−5985.
(40) Lee, M.; Cho, B.-K.; Zin, W.-C. Supramolecular Structures from Rod−Coil Block Copolymers. *Chem. Rev.* **2001**, *101*, 3869−3892.
(41) Xiao, L.-L.; Zhou, X.; Yue, K.; Guo, Z.-H. Synthesis and Self-Assembly of Conjugated Block Copolymers. *Polymers* **2021**, *13*, 110.
(42) Sugiyama, F.; Kleinschmidt, A. T.; Kayser, L. V.; Alkhadra, M. A.; Wan, J. M. H.; Chiang, A. S. C.; Rodriquez, D.; Root, S. E.; Savagatrup, S.; Lipomi, D. J. Stretchable and Degradable Semiconducting Block Copolymers. *Macromolecules* **2018**, *51*, 5944−5949.
(43) Müller, C.; Goffri, S.; Breiby, D. W.; Andreasen, J. W.; Chanzy, H. D.; Janssen, R. A. J.; Nielsen, M. M.; Radano, C. P.; Sirringhaus, H.; Smith, P.; Stingelin-Stutzmann, N. Tough, Semiconducting Polyethylene-Poly(3-Hexylthiophene) Diblock Copolymers. *Adv. Funct. Mater.* **2007**, *17*, 2674−2679.
(44) Peng, R.; Pang, B.; Hu, D.; Chen, M.; Zhang, G.; Wang, X.; Lu, H.; Cho, K.; Qiu, L. An Aba Triblock Copolymer Strategy for Intrinsically Stretchable Semiconductors. *J. Mater. Chem. C* **2015**, *3*, 3599−3606.
(45) Wang, J.-T.; Takshima, S.; Wu, H.-C.; Shih, C.-C.; Isono, T.; Kakuchi, T.; Satoh, T.; Chen, W.-C. Stretchable Conjugated Rod−Coil Poly(3-Hexylthiophene)-Block-Poly(Butyl Acrylate) Thin Films for Field Effect Transistor Applications. *Macromolecules* **2017**, *50*, 1442−1452.
(46) Ge, F.; Liu, Z.; Tian, F.; Du, Y.; Liu, L.; Wang, X.; Lu, H.; Wu, Z.; Zhang, G.; Qiu, L. One-Pot Synthesized Aba Tri-Block Copolymers for High-Performance Organic Field-Effect Transistors. *Polym. Chem.* **2018**, *9*, 4517−4522.
(47) Higashihara, T.; Fukuta, S.; Ochiai, Y.; Sekine, T.; Chino, K.; Koganezawa, T.; Osaka, I. Synthesis and Deformable Hierarchical Nanostructure of Intrinsically Stretchable Aba Triblock Copolymer Composed of Poly(3-Hexylthiophene) and Polyisobutylene Segments. *ACS Appl. Polym. Mater.* **2019**, *1*, 315−320.
(48) Hsu, L.-C.; Kobayashi, S.; Isono, T.; Chiang, Y.-C.; Ree, B. J.; Satoh, T.; Chen, W.-C. Highly Stretchable Semiconducting Polymers for Field-Effect Transistors through Branched Soft−Hard−Soft Type Triblock Copolymers. *Macromolecules* **2020**, *53*, 7496−7510.
(49) Yu, X.; Xiao, K.; Chen, J.; Lavrik, N. V.; Hong, K.; Sumpter, B. G.; Geohegan, D. B. High-Performance Field-Effect Transistors Based on Polystyrene-B-Poly(3-Hexylthiophene) Diblock Copolymers. *ACS Nano* **2011**, *5*, 3559−3567.
(50) Lee, J.-Y.; Lin, C.-J.; Lo, C.-T.; Tsai, J.-C.; Chen, W.-C. Synthesis, Morphology, and Field-Effect Transistor Characteristics of Crystalline Diblock Copolymers Consisted of Poly(3-Hexylthiophene) and Syndiotactic Polypropylene. *Macromolecules* **2013**, *46*, 3005−3014.
(51) Miyane, S.; Wen, H.-F.; Chen, W.-C.; Higashihara, T. Synthesis of Block Copolymers Comprised of Poly(3-Hexylthiophene) Segment with Trisiloxane Side Chains and Their Application to Organic Thin Film Transistor. *J. Polym. Sci., Part A: Polym. Chem.* **2018**, *56*, 1787−1794.
(52) Beck, J. B.; Ineman, J. M.; Rowan, S. J. Metal/Ligand-Induced Formation of Metallo-Supramolecular Polymers. *Macromolecules* **2005**, *38*, 5060−5068.
(53) Zhu, Y.; Zheng, W.; Wang, W.; Yang, H.-B. When Polymerization Meets Coordination-Driven Self-Assembly: Metallo-Supramolecular Polymers Based on Supramolecular Coordination Complexes. *Chem. Soc. Rev.* **2021**, *50*, 7395−7417.
(54) Zheng, B.; Hou, Y.; Gao, L.; Zhang, M. Luminescent Metallo-Supramolecular Polymers. *Chin. J. Chem.* **2019**, *37*, 843−854.
(55) Wu, H.-C.; Rondeau-Gagné, S.; Chiu, Y.-C.; Lissel, F.; To, J. W. F.; Tsao, Y.; Oh, J. Y.; Tang, B.; Chen, W.-C.; Tok, J. B. H.; Bao, Z. Enhanced Charge Transport and Stability Conferred by Iron(III)-Coordination in a Conjugated Polymer Thin-Film Transistors. *Adv. Electron. Mater.* **2018**, *4*, 1800239.
(56) Onge, P. B. J. St.; Chen, T.-C.; Langlois, A.; Younus, A.; Jo Hai, I.; Lin, B.-H.; Chiu, Y.-C.; Rondeau-Gagné, S. Iron-Coordinating Π-Conjugated Semiconducting Polymer: Morphology and Charge Transport in Organic Field-Effect Transistors. *J. Mater. Chem. C* **2020**, *8*, 8213−8223.
(57) He, Y.-J.; Tu, T.-H.; Su, M.-K.; Yang, C.-W.; Kong, K. V.; Chan, Y.-T. Facile Construction of Metallo-Supramolecular Poly(3-Hexylthiophene)-Block-Poly(Ethylene Oxide) Diblock Copolymers Via Complementary Coordination and Their Self-Assembled Nanostructures. *J. Am. Chem. Soc.* **2017**, *139*, 4218−4224.
(58) Tu, T.-H.; Sakurai, T.; Seki, S.; Ishida, Y.; Chan, Y.-T. Towards Macroscopically Anisotropic Functionality: Oriented Metallo-Supramolecular Polymeric Materials Induced by Magnetic Fields. *Angew. Chem., Int. Ed.* **2021**, *60*, 1923−1928.
(59) Lin, P.-S.; Shoji, Y.; Afraj, S. N.; Ueda, M.; Lin, C.-H.; Inagaki, S.; Endo, T.; Tung, S.-H.; Chen, M.-C.; Liu, C.-L.; Higashihara, T. Controlled Synthesis of Poly[(3-Alkylthio)Thiophene]S and Their Application to Organic Field-Effect Transistors. *ACS Appl. Mater. Interfaces* **2021**, *13*, 31898−31909.
(60) Tu, T.-H.; Chan, Y.-T. Synthesis of Terpyridine End-Modified Polystyrenes through Atrp for Facile Construction of Metallo-Supramolecular P3ht-B-Ps Diblock Copolymers. *Polymers* **2020**, *12*, 2842.
(61) Koch, F. P. V.; Rivnay, J.; Foster, S.; Müller, C.; Downing, J. M.; Buchaca-Domingo, E.; Westacott, P.; Yu, L.; Yuan, M.; Baklar, M.; Fei, Z.; Luscombe, C.; McLachlan, M. A.; Heeney, M.; Rumbles,

https://doi.org/10.1021/acs.macromol.2c00957
Macromolecules 2022, 55, 10670−10681

G.; Silva, C.; Salleo, A.; Nelson, J.; Smith, P.; Stingelin, N. The Impact of Molecular Weight on Microstructure and Charge Transport in Semicrystalline Polymer Semiconductors—Poly(3-Hexylthiophene), a Model Study. *Prog. Polym. Sci.* **2013**, *38*, 1978—1989.
(62) Alizadehaghdam, M.; Heck, B.; Siegenführ, S.; Abbasi, F.; Reiter, G. Thermodynamic Features of Perfectly Crystalline Poly(3-Hexylthiophene) Revealed through Studies of Imperfect Crystals. *Macromolecules* **2019**, *52*, 2487—2494.
(63) Lo, C.-T.; Lin, C.-J.; Lee, J.-Y.; Tung, S.-H.; Tsai, J.-C.; Chen, W.-C. Molecular Stacking Structure and Field-Effect Transistor Characteristics of Crystalline Poly(3-Hexylthiophene)-Block-Syndiotactic Polypropylene through Solvent Selectivity. *RSC Adv.* **2014**, *4*, 23002—23009.
(64) Spano, F. C.; Silva, C. H- and J-Aggregate Behavior in Polymeric Semiconductors. *Annu. Rev. Phys. Chem.* **2014**, *65*, 477—500.
(65) Wang, H.; Xu, Y.; Yu, X.; Xing, R.; Liu, J.; Han, Y. Structure and Morphology Control in Thin Films of Conjugated Polymers for an Improved Charge Transport. *Polymers* **2013**, *5*, 1272.
(66) Lenz, J.; Weitz, R. T. Charge Transport in Semiconducting Polymers at the Nanoscale. *APL Mater.* **2021**, *9*, 110902.
(67) Lin, J.-C.; Lee, W.-Y.; Kuo, C.-C.; Li, C.; Mezzenga, R.; Chen, W.-C. Synthesis, Morphology, and Field-Effect Transistor Characteristics of New Crystalline—Crystalline Diblock Copolymers of Poly(3-Hexylthiophene-Block-Steryl Acrylate). *J. Polym. Sci., Part A: Polym. Chem.* **2012**, *50*, 686—695.
(68) Linghu, C.; Zhang, S.; Wang, C.; Song, J. Transfer Printing Techniques for Flexible and Stretchable Inorganic Electronics. *npj Flexible Electron.* **2018**, *2*, 26.
(69) O'Connor, B.; Chan, E. P.; Chan, C.; Conrad, B. R.; Richter, L. J.; Kline, R. J.; Heeney, M.; McCulloch, I.; Soles, C. L.; DeLongchamp, D. M. Correlations between Mechanical and Electrical Properties of Polythiophenes. *ACS Nano* **2010**, *4*, 7538—7544.

https://doi.org/10.1021/acs.macromol.2c00957
Macromolecules 2022, 55, 10670—10681